Opto-Electronic Advances

ISSN 2096-4579 CN 51-1781/TN

Wide-spectrum optical synthetic aperture imaging via spatial intensity interferometry

Chunyan Chu, Zhentao Liu, Mingliang Chen, Xuehui Shao, Guohai Situ, Yuejin Zhao and Shensheng Han

Citation: Chu CY, Liu ZT, Chen ML, Shao XH, Situ GH et al. Wide-spectrum optical synthetic aperture imaging via spatial intensity interferometry. *Opto-Electron Adv* **6**, 230017(2023).

https://doi.org/10.29026/oea.2023.230017

Received: 8 February 2023; Accepted: 6 March 2023; Published online: 10 March 2023

Opto-Electronic Advances

Article

December 2023, Vol. 6, No. 12

DOI: 10.29026/oea.2023.230017

Wide-spectrum optical synthetic aperture imaging via spatial intensity interferometry

Chunyan Chu[1,2], Zhentao Liu[3,4]*, Mingliang Chen[3,4]*, Xuehui Shao[5], Guohai Situ[3,4], Yuejin Zhao[1,2] and Shensheng Han[3,6]

High resolution imaging is achieved using increasingly larger apertures and successively shorter wavelengths. Optical aperture synthesis is an important high-resolution imaging technology used in astronomy. Conventional long baseline amplitude interferometry is susceptible to uncontrollable phase fluctuations, and the technical difficulty increases rapidly as the wavelength decreases. The intensity interferometry inspired by HBT experiment is essentially insensitive to phase fluctuations, but suffers from a narrow spectral bandwidth which results in a lack of effective photons. In this study, we propose optical synthetic aperture imaging based on spatial intensity interferometry. This not only realizes diffraction-limited optical aperture synthesis in a single shot, but also enables imaging with a wide spectral bandwidth, which greatly improves the optical energy efficiency of intensity interferometry. And this method is insensitive to the optical path difference between the sub-apertures. Simulations and experiments present optical aperture synthesis diffraction-limited imaging through spatial intensity interferometry in a 100 nm spectral width of visible light, whose maximum optical path difference between the sub-apertures reaches 69λ. This technique is expected to provide a solution for optical aperture synthesis over kilometer-long baselines at optical wavelengths.

Keywords: optical synthetic aperture imaging; ghost imaging; intensity interferometry

Chu CY, Liu ZT, Chen ML, Shao XH, Situ GH et al. Wide-spectrum optical synthetic aperture imaging via spatial intensity interferometry. *Opto-Electron Adv* **6**, 230017 (2023).

Introduction

Intensity interferometry[1] performed by Robert Hanbury Brown and Richard Twiss in 1956 not only ushered in the era of quantum optics, but also provided a new approach for long baseline imaging[2]. Because conventional long baseline amplitude interferometry is susceptible to phase fluctuations, its phase error must be corrected, and the technical difficulty increases rapidly as the wavelength decreases. In contrast to amplitude interferometry, intensity interferometry is essentially insensitive to phase fluctuations, therefore, it enables very long baselines to be observed at shorter optical wavelengths with higher resolution. From 1964 to 1972, the Narrabri Stellar Intensity Interferometer (NSII) first measured the angular diameters of 32 stars using two 6.5 m reflectors on a circular track with a diameter of 188 m[3]. In HBT intensity interferometry, the intensity interferometer observes the second-order coherence of light by measuring

[1]Beijing Key Laboratory for Precision Optoelectronic Measurement Instrument and Technology, Beijing 100081, China; [2]School of Optics and Photonics, Beijing Institute of Technology, Beijing 100081, China; [3]Shanghai Institute of Optics and Fine Mechanics, Chinese Academy of Sciences, Shanghai 201800, China; [4]University of Chinese Academy of Sciences, Beijing 100049, China; [5]National Laboratory of Aerospace Intelligent Control Technology, Beijing 100089, China; [6]Hangzhou Institute for Advanced Study, University of Chinese Academy of Sciences, Hangzhou 310024, China.

*Correspondence: ZT Liu, E-mail: ztliu@siom.ac.cn; ML Chen, E-mail: cml2008@siom.ac.cn

Received: 8 February 2023; Accepted: 6 March 2023; Published online: 10 March 2023

the temporal correlations of the light intensity with different arrival times between photons recorded by different telescopes. Because the temporal coherence of light is determined by its bandwidth, the imaging bandwidth of this method is severely limited when recording the temporal intensity fluctuations of light. Owing to the lack of sensitivity[3], stellar intensity interferometry was almost abandoned in the 1970s[4]. With the significant development of light detectors (such as single photon avalanche diodes, SPADs) and signal processing, stellar intensity interferometry has attracted the interest of researchers' again[5–9]. S. Le Bohec et al. used ground-based Very High Energy gamma-ray observatories consist of arrays of up to four large (>12 m diameter) light collectors realized stellar intensity interferometry[10]. The major international project CTA[11] and Advanced Gamma-ray Imaging System AGIS[12] plan use 50–100 Cherenkov telescope arrays with aperture between 5 m and 25 m, distributed in the range of 1 to 2 square kilometers, to realize the measurement accuracy of sub-milliarcseconds stellar intensity interferometry. However, the lack of wide-spectrum optical synthetic aperture imaging has not been fundamentally solved.

Recent exciting advances in computational imaging have provided a new approach to far-field high-resolution imaging[13–19]. Novel research reported by Bulbul et al.[14] realized synthetic aperture-based imaging using coded phase reflectors distributed only along the boundaries of synthetic apertures. The image is obtained using cross-correlation between the detected system response to the object and system impulse response. However, this approach, which requiring a system impulse response, is limited to scenarios in which a guide-star is unobtainable. Inspired by ghost imaging using thermal light based on spatial intensity multi-correlation[20,21], Liu et al.[15] proposed a lensless Wiener-Khinchin telescope based on spatial intensity autocorrelation, which can acquire an image via a spatial random phase modulator in a snapshot. However, the requirement for a large aperture monolithic spatial random phase modulator with a statistical distribution restricts this approach to up to aperture imaging ten or even hundred meters.

In this study, we present a technique that enables wide-spectrum optical synthetic aperture imaging via spatial intensity interferometry in a single shot by combining light from Wiener-Khinchin telescopes separated by baselines. We verified that it can achieve a coherent synthetic aperture diffraction-limited resolution determined by the baseline length. Specifically, the energy spectral density of an object's image can be estimated using the intensity autocorrelation of the detected light, and the object's image can be reconstructed using phase retrieval algorithms[22–28]. As a proof of concept, we simulated and experimentally demonstrated wide-spectrum optical synthetic aperture imaging using a sub-aperture spatial random phase modulators (SRPMs) array.

Principle

A schematic of optical synthetic aperture imaging via spatial intensity interferometry is presented in Fig. 1. An object is placed at distance z_1 before the sub-aperture SRPMs array. The object is illuminated by spatially incoherent, narrowband thermal light, and a planar array light intensity detector (such as CCD and CMOS) that is placed at a distance z_2 behind the sub-aperture SRPMs array records the spatial intensity distribution of light that diffuses through the sub-aperture SRPMs array.

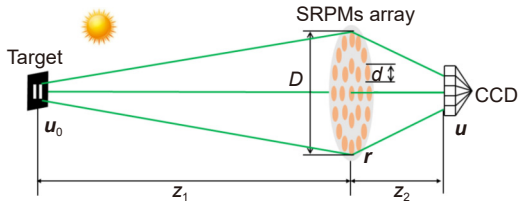

Fig. 1 | Schematic of wide-spectrum optical synthetic aperture imaging via spatial intensity interferometry.

In the field of view (FOV) within the memory-effect range (i.e., space translation invariance)[29–31], the detected intensity distribution is

$$I_{\rm t}(\boldsymbol{u}) = \int_{-\infty}^{\infty} I_0(\boldsymbol{u}_0) h_{\rm I}(\boldsymbol{u}-\boldsymbol{u}_0)\mathrm{d}\boldsymbol{u}_0 = I_0(\boldsymbol{u}) \otimes h_{\rm I}(\boldsymbol{u}) \ , \quad (1)$$

where $\otimes$ is the convolution operation, I_0 is the distribution of the object, $h_{\rm I}$ is the incoherent intensity impulse response function,

$$h_{\rm I}(\boldsymbol{u}) = |h_{\rm E}(\boldsymbol{u})|^2 = \left| \int_{-\infty}^{\infty} W(k) h_{\rm E}(\boldsymbol{u}, k)\mathrm{d}k \right|^2 , \quad (2)$$

where $h_{\rm E}(\boldsymbol{u})$ is the point-spread function (PSF), $h_{\rm E}(\boldsymbol{u}, k)$ is the PSF for the wave number $k = 1/\lambda$ (λ is the lambda), $W(k)$ is the detected spectral distribution of the wide spectrum.

According to the autocorrelation theorem and the convolution theorem[32], the spatial intensity autocorrelation of the detected light is

$$\begin{aligned} G_{I_t}^{(2)}(\Delta\boldsymbol{u}) &= \langle I_t(\boldsymbol{u}) I_t(\boldsymbol{u}+\Delta\boldsymbol{u})\rangle_{\boldsymbol{u}} \\ &= \int_{-\infty}^{\infty} I_t(\boldsymbol{u}) I_t(\boldsymbol{u}+\Delta\boldsymbol{u})\mathrm{d}\boldsymbol{u} \\ &= G_{I_0}^{(2)}(\Delta\boldsymbol{u}) \otimes G_{h_I}^{(2)}(\Delta\boldsymbol{u}) \,, \end{aligned} \tag{3}$$

where $\langle\cdot\rangle_{\boldsymbol{u}}$ is the spatial ensemble average over the coordinate $\boldsymbol{u}$, $G_{I_0}^{(2)}$and $G_{h_I}^{(2)}$ are the spatial intensity autocorrelation of object I_0 and the incoherent intensity impulse response function h_I, respectively.

We design the sub-aperture SRPMs obeys the following conditions (see Supplementary information for more details):

$$\text{Condition 1:}\quad D \ll \frac{8(n-1)z_2\sigma_\eta}{r_c} \,, \tag{4}$$

where D, n, σ_η and r_c are the synthetic aperture, the refractive index, the height variance and the transverse correlation length of the sub-aperture SRPMs, respectively. Meanwhile, the spectral width Δ_w of the detected spectral distribution W obeys

$$\begin{aligned} &\text{Condition 2:}\quad \Delta_w \ll \frac{1}{\sqrt{2}\pi(n-1)\sigma_\eta} \\ &\text{Condition 3:}\quad \Delta_w \ll \frac{2z_2}{DD_t} \,, \end{aligned} \tag{5}$$

where D_t is the detected width of CCD. Then, $G_{h_I}^{(2)}$ in Eq. (3) is given by

$$G_{h_I}^{(2)}(\Delta\boldsymbol{u}) \approx 1 + \left|\tau\mathfrak{F}_a\left(-\frac{k_0\Delta\boldsymbol{u}}{z_2}\right)\right|^2 \,, \tag{6}$$

where k_0 is the detected center wave number, $\mathfrak{F}_a$ is the Fourier transform function of the aperture function A, τ is the normalized factor.

Taking Eq. (6) into Eq. (3) yields

$$G_{I_t}^{(2)}(\Delta\boldsymbol{u}) = G_{I_0}^{(2)}(\Delta\boldsymbol{u}) \otimes \left\{1 + \left|\tau\mathfrak{F}_a\left(-\frac{k_0\Delta\boldsymbol{u}}{z_2}\right)\right|^2\right\} \,. \tag{7}$$

According to the Wiener–Khinchin theorem for deterministic signals (also known as the autocorrelation theorem)[32,33], we obtain $\mathfrak{F}\left\{G_I^{(2)}(\Delta\boldsymbol{u})\right\}_{\boldsymbol{r}} = \left|\mathfrak{F}\{I(\Delta\boldsymbol{u})\}_{\boldsymbol{r}}\right|^2$. Now applying the Fourier transform to Eq. (7) yields

$$\mathfrak{F}\left\{G_{I_t}^{(2)}(\Delta\boldsymbol{u})\right\}_{\boldsymbol{r}} = \left|\mathfrak{F}\{I_0(\Delta\boldsymbol{u})\}_{\boldsymbol{r}}\right|^2 \mathcal{H}(\boldsymbol{r}) + C \,, \tag{8}$$

where $C = \left\{\left|\mathfrak{F}\{I_0(\Delta\boldsymbol{u})\}_{\boldsymbol{r}}\right|^2\right\}\Big|_{\boldsymbol{r}=0}$ is a constant, and

$$\mathcal{H}(\boldsymbol{r})_{\boldsymbol{r}} = \int_{-\infty}^{\infty} A(\boldsymbol{r}_0) A\left(\boldsymbol{r}_0 + \frac{k_0\boldsymbol{r}}{z_2}\right)\mathrm{d}\boldsymbol{r}_0 \,, \tag{9}$$

is the autocorrelation of the synthetic aperture A, and the fact of A is an even function has been used to replace $A\left(-\boldsymbol{r}_0 - \frac{k_0\boldsymbol{r}}{z_2}\right)$ by $A\left(\boldsymbol{r}_0 + \frac{k_0\boldsymbol{r}}{z_2}\right)$.

Specially, the pupil function of synthetic aperture of the sub-aperture SRPMs array is expressed as $P(\boldsymbol{r}) = A(\boldsymbol{r})S(\boldsymbol{r})$, where $S(\boldsymbol{r})$ is the modulation phase transfer function of the sub-aperture SRPMs array, $A(\boldsymbol{r}) = \sum_{n=1}^{N} A_{\text{sub}}^{(n)}(\boldsymbol{r}) \otimes \delta(\boldsymbol{r} - \boldsymbol{r}_n)$ is the aperture function, $A_{\text{sub}}^{(n)}(\boldsymbol{r})$ and $\boldsymbol{r}_n$ are the aperture function and the position coordinates of sub-aperture SRPM n, respectively. N is the number of sub-aperture SRPMs, and $\delta(\cdot)$ is the Dirac function. To simplify the theoretical analysis, the aperture function of each sub-aperture SPRM is a circular aperture with the same diameter d, i.e., $A_{\text{sub}}^{(n)}(\boldsymbol{r}) = A_{\text{sub}}(\boldsymbol{r})$, and

$$A(\boldsymbol{r}) = \sum_{n=1}^{N} A_{\text{sub}}(\boldsymbol{r}) \otimes \delta(\boldsymbol{r} - \boldsymbol{r}_n) \,. \tag{10}$$

Substituting this into Eq. (9) yields

$$\mathcal{H}(\boldsymbol{r}) = \frac{1}{N}\sum_{n=1}^{N}\sum_{m=1}^{N} \mathcal{H}_{\text{sub}}\left(\boldsymbol{r} - \frac{\Delta\boldsymbol{r}_{mn}}{\lambda z_2}\right) \,, \tag{11}$$

where $\Delta\boldsymbol{r}_{mn} = \boldsymbol{r}_m - \boldsymbol{r}_n$, and

$$\mathcal{H}_{\text{sub}}(\boldsymbol{r}) = \int_{-\infty}^{\infty} A_{\text{sub}}(\boldsymbol{r}_0) A_{\text{sub}}\left(\boldsymbol{r}_0 + \frac{\boldsymbol{r}}{\lambda z_2}\right)\mathrm{d}\boldsymbol{r}_0 \,, \tag{12}$$

is the sub-aperture's optical transfer function (OTF).

Thus, the diffraction-limited effects of the optical synthetic aperture imaging expressed in the frequency domain. Equation (8) shows the frequency spectra's modulus $\mathfrak{F}\{I_0(\Delta\boldsymbol{u})\}_{\boldsymbol{r}}$ of object's diffraction-limited image intensity I_0 can be estimated by the intensity autocorrelation $G_{I_t}^{(2)}$ of detected light intensity I_t, and then I_0 is reconstructed by phase retrieval algorithms[22–27]. As shown in Eq. (9), the frequency response of the optical synthetic aperture imaging is similar to that of the incoherent imaging case, and $\mathcal{H}$ is similar to the OTF of the incoherent imaging system. Therefore, the resolution of the object' is primarily determined by the baseline length D of the synthetic aperture. And according to the Rayleigh criterion of resolution, the angular resolution is limited to $1.22\lambda/D$ with a circular synthetic aperture[34]. Equation (11) represents the relationship between $\mathcal{H}$ and $\mathcal{H}_{\text{sub}}$, which is consistent with conventional synthetic aperture imaging[34]. Finally, note that the phase error ϕ_n of the sub-aperture can be placed in the modulation phase transfer function $S(\boldsymbol{r})$, and its effect is primarily reflected in its influence on the statistical characteristics of $S(\boldsymbol{r})$. Therefore, the wide-spectrum optical synthetic aperture imaging via spatial intensity interferometry is insensitive

to the phase error and turbulence-free in the case of the statistical conditions in Eqs. (4, 5) satisfied with phase error or turbulence.

For traditional optical synthetic aperture systems, according to the illumination source, it can be classified to two categories: traditional active optical synthetic aperture methods such as Fourier ptychography imaging[35] method or synthetic aperture lidar[36], and traditional passive optical synthetic aperture systems. In traditional passive optical synthetic aperture systems, if we seek to achieve the imaging resolution by synthetic aperture[34], not only the optical path difference ΔL between different lights L_{11} and L_{12} of a single aperture must be less than $\lambda/4$, but also the optical path difference between sub-apertures M_1, M_2, M_3 must be less than $\lambda/4$, as shown in Fig. 2. To achieve the imaging resolution limit of a very large telescope interferometer (VLTI) system[37], the optical path difference between sub-apertures is controlled below $\lambda/20$ using delay lines. But in the method presented in this study, the optical path difference between sub-apertures S_1, S_2, and S_3 can also be included in $S(\boldsymbol{r})$. The theoretical analysis shows that the imaging resolution is limited by the baseline length of the synthetic aperture.

Compared with stellar intensity interferometry using temporal intensity correlations, which severely limits the imaging bandwidth and sensitivity, a major advantage of the presented approach is that it does not require measuring temporal correlations of light intensity with different arrival times between photons recorded in different telescopes, and the imaging bandwidth is limited by chromatic dispersion, which required to satisfy the conditions in Eq. (5), not by recording the temporal intensity fluctuations of light. The optical energy efficiency of wide-spectrum optical synthetic aperture imaging is significantly improved with this approach.

The imaging structure of this approach is reminiscent of a synthetic marginal aperture with revolving telescopes (SMART)[14], however, unlike SMART, it does not require a long invasive calibration procedure involving a guide-star to measure the system impulse response and is insensitive to atmospheric turbulence. Similar to stellar speckle interferometry, single-shot imaging through scattering media and the Wiener-Khinchin telescope, the object's image is recovered from spatial intensity autocorrelation. However, in the present approach the autocorrelation of an object's image is obtained from a single image via spatial ensemble averaging, where a stellar speckle interferometry obtains the autocorrelation of an object's image from multiple images via temporal ensemble averaging. Compared with single-shot imaging through scattering media and the Wiener-Khinchin telescope through a monolithic spatial random phase modulator, this technique is modulated by the sub-aperture SRPMs array and its diffraction is limited by the length of the baseline of the sub-aperture SRPMs array. The angular FOV of this approach is limited by the memory effect range through the sub-aperture SRPMs array, which is inversely proportional to the SPRMs' height standard deviation of the sub-aperture array[15].

Simulation and experiment

A schematic diagram of the simulation is shown in Fig. 3(a). The distance z_1 from the target to the SRPMs array was 2.00 m. The distance z_2 from the SRPMs to CCD was 0.34 m. The structure of the SRPMs array is shown in Fig. 3(b). The diameter d of the sub-aperture was 1 mm. The length of the baseline of the synthetic aperture D was 10 mm. Independent spatial random phase modulators were used for each sub-aperture. In the simulation, the number of CCD pixels was 512×512, and the pixel size was 4.4 μm.

The optical path structure of the experiment is shown in Fig. 3(c). The main parameters of the experiment were consistent with those of the simulation, except those two mirrors were inserted into the optical path, where $L_1 + L_2 + L_3 = z_1$. To produce a light source with good directionality, light was generated using a super-continuous laser through rotating glass in the experiment. The

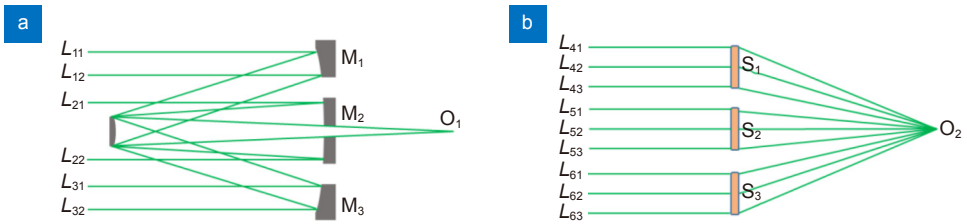

Fig. 2 | (**a**) Traditional optical synthetic aperture system. (**b**) Schematic of wide-spectrum optical synthetic aperture imaging via spatial intensity interferometry.

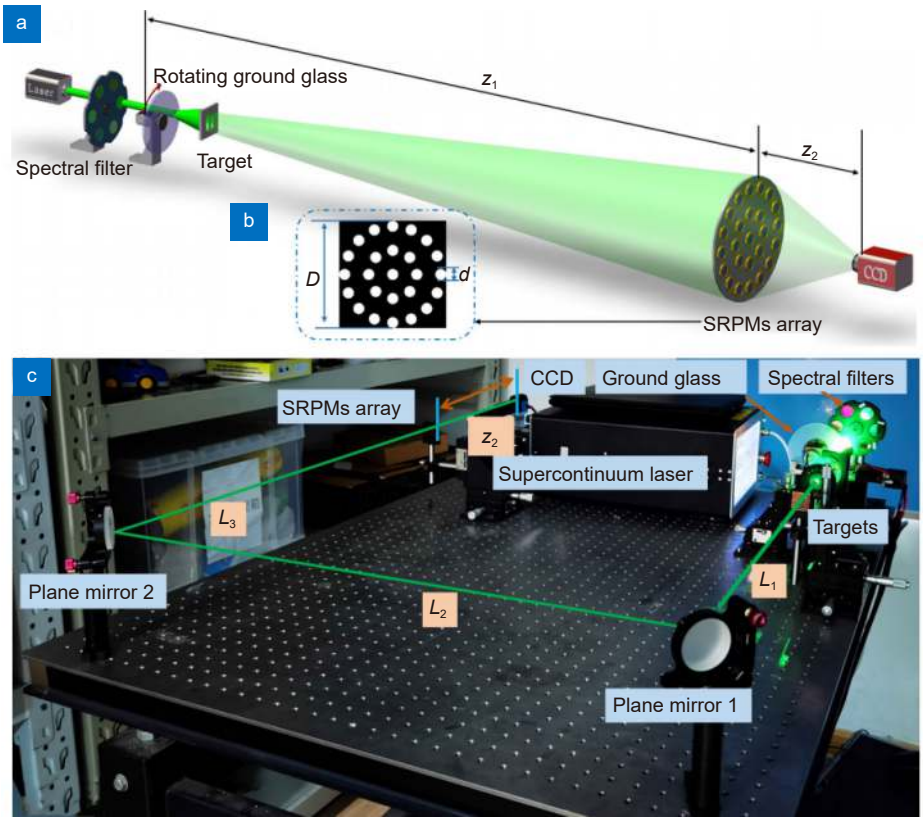

Fig. 3 | (**a**) Schematic diagram of the simulation structure. (**b**) Structure of sub-aperture SRPMs array. (**c**) Optical path structure of the experiment.

pseudothermal light generated by this method has the same characteristics as real thermal light[15]. The spectral width of the supercontinuum laser ranged from 430 nm to 2400 nm. The size of the laser spot on the ground glass surface was approximately 4 mm. The speed of the rotating ground glass was approximately 120–180 r/min. The number of pixels for the sampling CCD were 1600×1200, 512×512 pixels in the central area are selected for reconstruction calculation.

To test the imaging resolution, we selected double slits as the target in the simulation and experiment. The center distances Δx of the double-slit were 130 μm, 195 μm and 260 μm, respectively; they were 1.0, 1.5 and 2.0 times the diffraction limit $(1.22\lambda z_1/D)$ of the synthetic aperture, respectively (Fig. 4(a1–c1)). Figure 4(a4) and 4(a7) show the one-dimensional normalized date of double slits reconstruction images, the results show that the resolution limit of simulation and experiment both consistent with the theory. When the distances of the double-slits were wider than the diffraction limit, they could be clearly distinguished, as shown in Fig. 4(b4, c4, b7, c7). Therefore, the optical synthetic aperture using a sub-aperture SRPMs array has the same imaging resolution as the full aperture system.

Optical synthetic aperture imaging via spatial intensity interferometry has another advantage: it can realize wideband spectrum optical intensity interference imaging. The simulation and experimental results are shown in Fig. 5. We used spectral filters to select the wavelengths of the light source. The spectral ranges of the filters were 532±5 nm, ±10 nm, ±15 nm, ±25 nm, ±50 nm, respectively. The target was a double-slit whose center distance Δx of slits is 130 μm. The single-shot imaging detected using the CCD is shown in Fig. 5(1, 4); the contrast of images decreased with the increase in spectral width. However, the resolution of the image increased with the spectral width, as shown in Fig. 5(3, 6). This may have been due to the shorter-wavelength components with a wider spectral width. For example, when the spectral width was 532±50 nm, the shortest wavelength was 482 nm. When z_1=2.00 m, the imaging resolution of the system was 118 μm, which was shorter than 130 μm. Both the simulation and experimental results verified that optical synthetic aperture imaging via spatial intensity interferometry can be used for imaging with a wide spectral width. Compared with traditional coherent synthetic aperture optical intensity interference imaging, the detection sensitivity of this system is

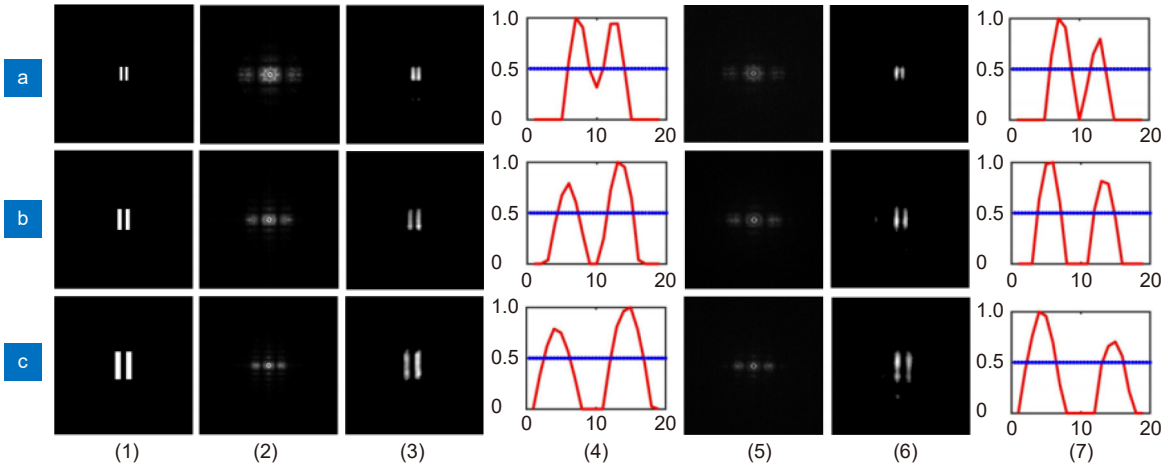

Fig. 4 | Simulation and experimental results. The spectral widths of the filters were 532 ± 0.5 nm. (**a1**–**c1**) Targets. (**2**–**4**) Simulation results. (**5**–**7**) Experimental results. In the experiment, the exposure times of CCD were 1.2 s, 0.75 s, 0.5 s, and the gains of CCD were 30 dB, 30 dB, 28 dB, respectively. (2, 5) Spatial intensity autocorrelation of CCD. (3, 6) Reconstruction of target image using phase retrieval algorithms. (4, 7) One-dimensional normalized date of double slits reconstruction image. The blue lines indicate half of the maximum value.

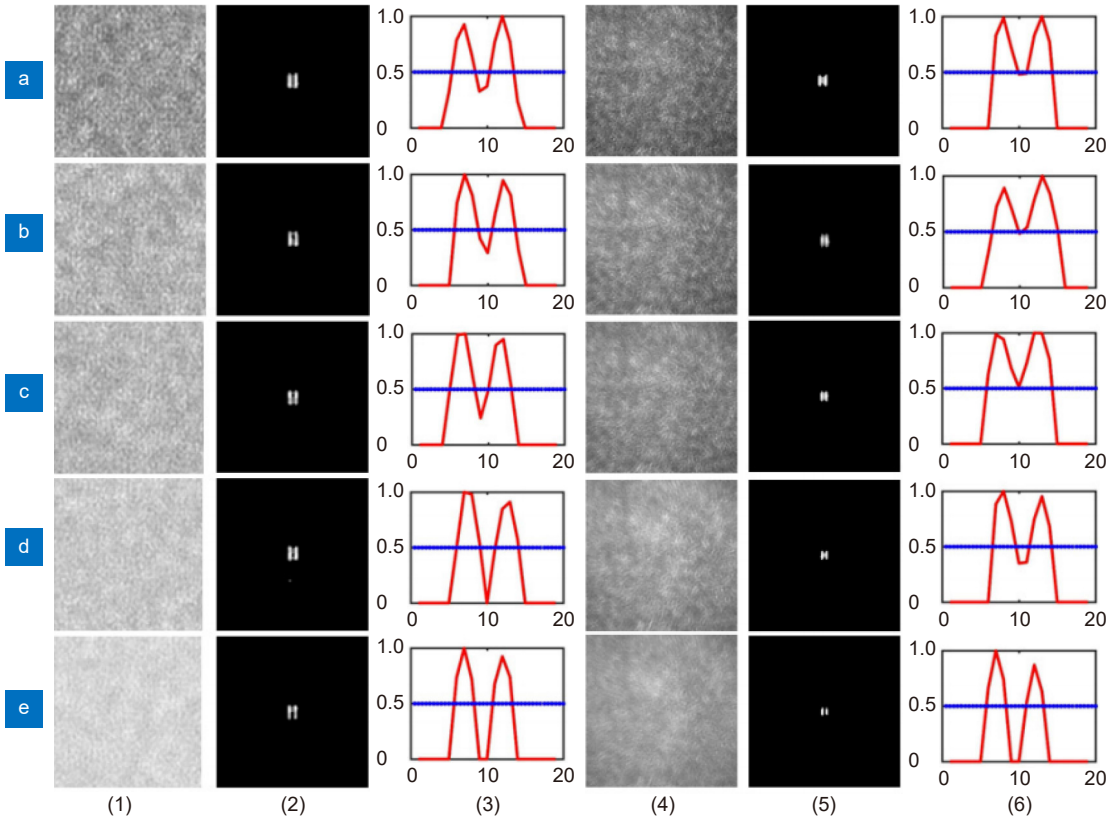

Fig. 5 | Simulation and experimental results of wide-spectrum optical synthetic aperture imaging via spatial intensity interferometry. (**a**–**e**) The spectral ranges of the filters were 532 ±5 nm, ±10 nm, ±15 nm, ±25 nm, ±50 nm, respectively. (**1**–**3**) Simulation results. (**4**–**6**) Experimental results. The sampling exposure times of CCD were 250 ms, and the gains of CCD were 9 dB, 16 dB, 23 dB, 25 dB, 30 dB, respectively. (1, 4) The detected image by CCD. (2, 5) Reconstruction of target image using phase retrieval algorithms. (3, 6) One-dimensional normalized date of double slits reconstruction image. The blue lines indicate half of the maximum value.

significantly improved owing to the increase in spectral width.

A special sub-aperture structure was designed for simulation and experiment, as shown in Fig. 3(b). To test the imaging effect of different sparse array structures, we designed a full aperture and other structures designed for comparative experiments, as shown in Fig. 6(a). The experimental results show that the imaging resolution of the synthetic aperture system was maintained, but the imaging quality of sparse array structures was not as high as that of a full aperture structure, because synthetic apertures are sparse array structures, which have the problem of frequency spectrum loss. The Fourier transform of the full circular aperture structure is the 1th Bessel function[34], but the Fourier transform of sparse array structures are accompanied by strong sidelobes[38], as shown in Fig. 6(b). Therefore, using a sparse array structure synthetic aperture to sample has the problems of missing information and sidelobe disturbance. Then, the sparse array structure should be optimized according to specific objectives and application scenarios.

Discussion and conclusion

In this paper, we propose a wide-spectrum optical synthetic aperture imaging via spatial intensity interferometry. Different sub-aperture spatial random phase modulators arrays and the imaging spectrum widths are analyzed. Optical synthetic aperture imaging via spatial intensity interferometry can overcome the high time coherence and narrow-band spectral width required by the traditional intensity interference imaging. When the diameter D of the synthetic aperture is 10 mm and z_2 is 0.34 m, the optical path difference between the center light L_{52} and the edge light L_{41} is 37 μm, which is equivalent to 69λ when the central wavelength is 532 nm and much larger than $\lambda/4$, as shown in Fig. 2. Therefore, the optical synthetic aperture imaging mentioned in this study is insensitive to the optical path difference between the sub-apertures, which significantly reduces the difficulty of synthetic aperture construction.

In addition, in the experiment and simulation, the spectral width of the system reached 100 nm, which significantly improved the detection sensitivity of the system. In principle, this method is not limited to the width of the spectrum, but a spectrum that is too wide will significantly reduce the contrast of the detected image using CCD. If we want to realize the effective detection of wide-band intensity interferometry, the dynamic range

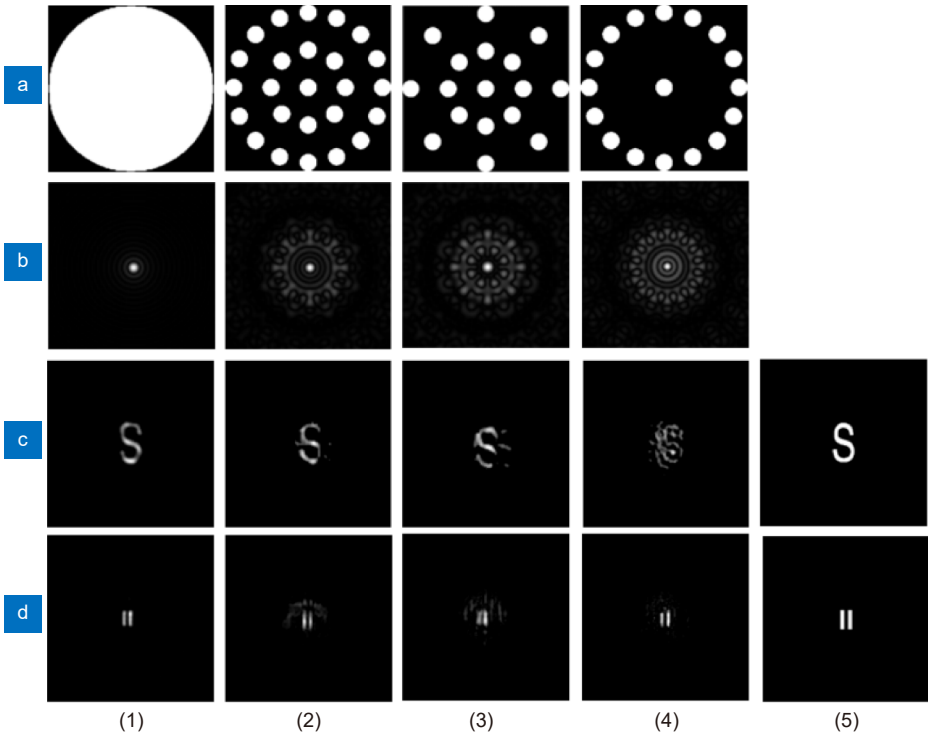

Fig. 6 | Experimental results of different sub-aperture SRPMS arrays. (**a**) Different sparse array structures. (**b**) Spatial intensity autocorrelation of different sparse array structures. (**c1**–**c4**) Reconstruction of 's' image using phase retrieval algorithms by different sparse array structures. (**d1**–**d4**) Reconstruction of double-slit image using phase retrieval algorithms by different sparse array structures. (**5**) Target letter 's' and double-slit, whose sizes were 2.0 mm and 0.98 mm, respectively.

of the detector CCD must be sufficiently high to satisfy the requirements of data acquisition.

This study provided a possible solution to reducing the construction difficulty of optical synthetic aperture telescopes and increasing the baseline length of optical telescope to 100 m or even kilometers. Wide-spectrum optical synthetic aperture imaging via spatial intensity interferometry has potential application value in astronomical observation and space target high-resolution imaging. Recently, astronomers have shown the first picture of a supermassive black hole in the center of the Milky Way galaxy, which is an important proof of the resolution advantage of the synthetic aperture telescope in astronomical observation[39].

References

1. Brown RH, Twiss RQ. Correlation between photons in two coherent beams of light. *Nature* **177**, 27–29 (1956).
2. Twiss RQ. Applications of intensity interferometry in physics and astronomy. *Opt Acta Int J Opt* **16**, 423–451 (1969).
3. Brown RH, Davis J, Allen LR. The angular diameters of 32 stars. *Mon Not Roy Astron Soc* **167**, 121–136 (1974).
4. Rivet JP, Vakili F, Lai O, Vernet D, Fouché M et al. Optical long baseline intensity interferometry: prospects for stellar physics. *Exp Astron* **46**, 531–542 (2018).
5. Nuñez PD, Holmes R, Kieda D, LeBohec S. High angular resolution imaging with stellar intensity interferometry using air cherenkov telescope arrays. *Mon Not Roy Astron Soc* **419**, 172–183 (2012).
6. Pilyavsky G, Mauskopf P, Smith N, Schroeder E, Sinclair A et al. Single-photon intensity interferometry (SPIIFy): utilizing available telescopes. *Mon Not Roy Astron Soc* **467**, 3048–3055 (2017).
7. Gori PM, Vakili F, Rivet JP, Guerin W, Hugbart M et al. I3T: intensity interferometry imaging telescope. *Mon Not Roy Astron Soc* **505**, 2328–2335 (2021).
8. Xu BX, Fan XY, Wang S, He ZY. Sub-femtometer-resolution absolute spectroscopy with sweeping electro-optic combs. *Opto-Electron Adv* **5**, 210023 (2022).
9. Li CL, Liu JC, Zhang FM Qu XH. Review of nonlinearity correction of frequency modulated continuous wave LiDAR measurement technology. *Opto-Electron Eng* **49**, 210438 (2022).
10. Le Bohec S, Daniel M, de Wit WJ, Hinton JA, Jose E et al. Stellar intensity interferometry with air Cherenkov telescope arrays. *AIP Conf Proc* **984**, 205–215 (20008).
11. Dravins D, LeBohec S, Jensen H, Nuñez PD. Stellar intensity interferometry: prospects for sub-milliarcsecond optical imaging. *New Astron Rev* **56**, 143–167 (2012).
12. Buckley J, Coppi P, Digel S, Funk S, Krawczynski H et al. The Advanced Gamma - ray Imaging System (AGIS) —Science Highlights. *AIP Conf Proc* **1085**, 902–905 (2008).
13. Gong WL, Han SS. High-resolution far-field ghost imaging via sparsity constraint. *Sci Rep* **5**, 9280 (2015).
14. Bulbul A, Vijayakumar A, Rosen J. Superresolution far-field imaging by coded phase reflectors distributed only along the boundary of synthetic apertures. *Optica* **5**, 1607–1616 (2018).
15. Liu ZT, Shen X, Liu HL, Yu H, Han SS. Lensless wiener–khinchin telescope based on second-order spatial autocorrelation of thermal light. *Chin Opt Lett* **17**, 091101 (2019).
16. Bulbul A, Rosen J. Super-resolution imaging by optical incoherent synthetic aperture with one channel at a time. *Photonics Res* **9**, 1172–1181 (2021).
17. Wang F, Wang CL, Chen ML, Gong WL, Zhang Y et al. Far-field super-resolution ghost imaging with a deep neural network constraint. *Light Sci Appl* **11**, 1–11 (2022).
18. Liu YL, Chen YH, Wang F, Cai YJ, Liang CH et al. Robust far-field imaging by spatial coherence engineering. *Opto-Electron Adv* **4**, 210027 (2021).
19. Hu Y, Xiang HZ, Zhao RY, Tu JK, Zheng G. Mode field diameter measurement of single mode fiber using Bessel function fitting method based on variable aperture in far field. *Opto-Electron Eng* **48**, 200308 (2021).
20. Liu ZT, Tan SY, Wu JR, Li ER, Shen X et al. Spectral camera based on ghost imaging via sparsity constraints. *Sci Rep* **6**, 25718 (2016).
21. Chen SC, Du LH, Zhu LG. THz wave computational ghost imaging: principles and outlooks. *Opto-Electron Eng* **47**, 200024 (2020).
22. Fienup JR. Reconstruction of an object from the modulus of its Fourier transform. *Opt Lett* **3**, 27–29 (1978).
23. Fienup JR. Phase retrieval algorithms: a comparison. *Appl Opt* **21**, 2758–2769 (1982).
24. Liu XL, Wu JC, He WQ, Liao MH, Zhang CG et al. Vulnerability to ciphertext-only attack of optical encryption scheme based on double random phase encoding. *Opt Express* **23**, 18955–18968 (2015).
25. Shechtman Y, Eldar YC, Cohen O, Chapman HN, Miao JW et al. Phase retrieval with application to optical imaging: a contemporary overview. *IEEE Signal Process Mag* **32**, 87–109 (2015).
26. Sun J, Qu Q, Wright J. A geometric analysis of phase retrieval. *Found Comput Math* **18**, 1131–1198 (2018).
27. Shen C, Liang MS, Pan A, Yang C. Non-iterative complex wavefield reconstruction based on Kramers–Kronig relations. *Photonics Res* **9**, 1003–1012 (2021).
28. Liao MH, Zheng SS, Pan SX, Lu DJ, He WQ et al. Deep-learning-based ciphertext-only attack on optical double random phase encryption. *Opto-Electron Adv* **4**, 200016 (2021).
29. Feng SC, Kane C, Lee PA, Stone AD. Correlations and fluctuations of coherent wave transmission through disordered media. *Phys Rev Lett* **61**, 834–837 (1988).
30. Osnabrugge G, Horstmeyer R, Papadopoulos IN, Judkewitz B, Vellekoop IM. Generalized optical memory effect. *Optica* **4**, 886–892 (2017).
31. Wang XY, Jin X, Li JQ. Blind position detection for large field-of-view scattering imaging. *Photonics Res* **8**, 920–928 (2020).
32. Goodman JW. *Introduction to Fourier Optics* 3rd ed 7–9 (Roberts & Company Publishers, Greenwoood Village, 2005).
33. Cohen L. The generalization of the wiener-khinchin theorem. in *Proceedings of 1998 IEEE International Conference on Acoustics, Speech and Signal Processing* 1577–1580 (IEEE, 1998).
34. Saha SK. *Aperture Synthesis: Methods and Applications to Optical Astronomy* 28 (Springer, New York, 2010).
35. Zheng GA, Shen C, Jiang SW, Song PM, Yang C. Concept, implementations and applications of Fourier ptychography. *Nat Rev Phys* **3**, 207–223 (2021).
36. Bashkansky M, Lucke RL, Funk E, Rickard LJ, Reintjes J.

Two-dimensional synthetic aperture imaging in the optical domain. *Opt Lett* **27**, 1983–1985 (2002).
37. Derie F. VLTI delay lines: design, development, and performance requirements. *Proc SPIE* **40006**, 25–40 (2000).
38. Shannon RR, Wyant JC. *Applied Optics and Optical Engineering* 156–158 (Academic Press, 1983).
39. Event Horizon Telescope Collaboration, Akiyama K, Alberdi A, Alef W, Algaba JC et al. First Sagittarius A* event horizon telescope results. I. The shadow of the supermassive black hole in the center of the milky way. *Astrophys J Lett* **930**, L12 (2022).

Acknowledgements

This work is supported by National Natural Foundation of China (Grant No. 61991454) and the project of CAS Interdisciplinary Innovation Team. Thanks are due to Dr. Feng Lu (National Astronomical Observatory, Chinese Academy of Sciences) for valuable discussion about the optical synthetic aperture systems.

Author contributions

The scheme of optical synthetic aperture imaging via spatial intensity interferometry was proposed by S. S. Han, Z. T. Liu and M. L. Chen. The theoretical derivation was completed by Z. T. Liu and C. Y. Chu, with help from M. L. Chen, G. H. Situ and S. S. Han. The simulation and experiment were completed by M. L. Chen and C. Y. Chu, with help from Z. T. Liu, X. H. Shao and Y. J. Zhao. The manuscript was written by C.Y. Chu, Z. T. Liu and M. L. Chen. All the authors contributed to critical discussion of the results and contributed to write the manuscript. All authors agreed on the final content of the manuscript.

Competing interests

The authors declare no competing financial interests.

Supplementary information

See the supplementary material for the derivation of the incoherent intensity impulse response function's spatial intensity autocorrelation, the correlation of modulation phase transfer function, and the design conditions of sub-aperture spatial random phase modulators.
https://doi.org/10.29026/oea.2023.230017